and

$$\begin{aligned} N_{sm} \pm \kappa_1 v_m &= \tilde{N}_{sm} \\ N_m \pm \kappa_2 u_m &= \tilde{N}_m \\ M_{sm} \pm \kappa_3 w_{m,s} &= \tilde{M}_{sm} \\ Q_m \pm \kappa_4 w_m &= \tilde{Q}_m \end{aligned} \tag{21}$$

Contrary to the isotropic[9] or orthotropic cases, for nonzero E_{16} and E_{26}, Re $\{\xi_m\}$ and Im $\{\xi_m\}$ are coupled.

Irrespective of their complex form, the homogeneous solution of Eqs. (20 and 21) takes the form

$$\xi_m = \sum_{i=1}^{8} \alpha_{mi} \zeta_{mi} e^{\lambda_{mi} x} \tag{22}$$

where λ_{mi} and ζ_{mi} are latent roots and vectors of the following irregular complex fourth order polynomial matrix

$$\begin{aligned} &\{\lambda_{mi}^4 \mathbf{Q}_1 + \lambda_{mi}^3 [\mathbf{Q}_6 + jm\mathbf{Q}_2] + \lambda_{mi}^2 [\mathbf{Q}_{10} - m^2 \mathbf{Q}_3 + \\ &\quad jm\mathbf{Q}_7] + \lambda_{mi} [\mathbf{Q}_{13} - m^2 \mathbf{Q}_8 + j(m\mathbf{Q}_{11} - m^3 \mathbf{Q}_4)] + \\ &\quad [\mathbf{Q}_{15} + m^4 \mathbf{Q}_5 - m^2 \mathbf{Q}_{12} + j(m\mathbf{Q}_{14} - m^3 \mathbf{Q}_9)]\} \zeta_{mi} = \mathbf{0} \end{aligned} \tag{23}$$

By taking the determinant of the pencil of Eq. (23), the following complex characteristic polynomial is obtained

$$\sum_{i=0}^{8} g_i \lambda^{8-i} = 0 \tag{24}$$

such that g_i are complex constants. For the isotropic[9] and orthotropic cases, $g_1, g_3, \ldots, g_7$ reduce to zero. The constants α_{mi} appearing in Eq. (22) are obtained by satisfying the transformed boundary conditions denoted by Eq. (21).

Since Eq. (23) has a complex pencil, its latent roots and associated latent vectors no longer occur in conjugate pairs for a given m value. However, due to its inherent functional dependency, it follows from Eq. (23) that

$$\bar{\lambda}_{mi} = \lambda_{-mi} \tag{25}$$

and

$$\bar{\zeta}_{mi} = \zeta_{-mi} \tag{26}$$

Furthermore, based on the transformed boundary conditions and Eqs. (25 and 26), it also follows that

$$\bar{\alpha}_{mi} = \alpha_{-mi} \tag{27}$$

Hence, in terms of Eqs. (18, 22 and 25–27), ξ is given by

$$\begin{aligned} \xi = &\sum_{i=1}^{8} \alpha_{0i} \zeta_{0i} s^{\lambda_{0i}} + \\ &\sum_{m=1}^{\infty} \sum_{i=1}^{8} 2 [\mathrm{Re}(\alpha_{mi} \zeta_{mi}) \cos(\mathrm{Im}(\lambda_{mi}) \ln s + m\theta) - \\ &\quad \mathrm{Im}(\alpha_{mi} \zeta_{mi}) \sin(\mathrm{Im}(\lambda_{mi}) \ln s + m\theta)] s^{\mathrm{Re}(\lambda_{mi})} \end{aligned} \tag{28}$$

The inplane and bending resultant fields can be directly obtained by substituting Eq. (28) into Eqs. (2) and (3), respectively. Since the procedure used to develop the solution is basically an extension of the Levy technique used for classical isotropic and orthotropic problems, the convergence of Eq. (28) is directly dependent on the number of terms needed to represent the various boundary conditions and surface tractions in standard Fourier series.

Example

As an example of the possible effects of material anisotropy the following boundary value problem is considered

$$\begin{aligned} s = 15'' \text{ or } 36'' \qquad & u = v = w \equiv 0 \\ P_r = \sigma \cos\theta \qquad & P_\theta = P_s = 0 \end{aligned} \tag{29}$$

where $\alpha = 60°$, $\delta = 1/150$, and β the local material orientation depicted in Fig. 1 is chosen as either 0° or 45°. For the present study the latent roots and vectors of Eq. (23) were obtained by recasting Eq. (24) as a complex eigenvalue problem which can be solved using standard eigenvalue procedures.[1-3] The computational times needed to evaluate the said eigenvalue problems were essentially the same as those required to obtain the roots of classical isotropic and orthotropic problems.[9] Figure 2 presents

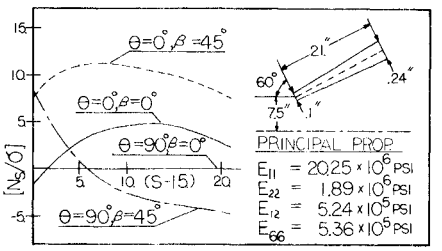

Fig. 2 Effects of β on N_s field of tapered cone.

the significant effects of α on the N_s field. Similar redistributions are also noted for the remaining field variables.

References

[1] Padovan, J., "Frequency and Buckling Eigenvalues of Anisotropic Cylinders Subjected to Nonuniform Lateral Prestress," *International Journal of Solids and Structures*, Vol. 7, 1971, pp. 1449–1466.

[2] Padovan, J. and Lestingi, J., "Mechanical Behavior of Fiber Reinforced Cylinders," *AIAA Journal*, Vol. 10, No. 9, Sept. 1972, pp. 1239–1241.

[3] Padovan, J., "Natural Frequencies of Rotating Prestressed Cylinders," *Journal of Sound and Vibration*, (in press, Dec. 1973).

[4] Padovan, J., "In Plane and Bending Fields of Anisotropic Generally Laminated Plate Strips," *Journal of Composite Materials* (in press).

[5] Padovan, J. and Lestingi, J., "Static Solution of Monoclinic Circular Plates," *AIAA Journal*, Vol. 9, No. 12, Dec. 1971, pp. 2473–2474.

[6] Padovan, J. and Lestingi, J., "Natural Frequencies of Monoclinic Circular Plates," *Journal of the Acoustical Society of America*, to be published.

[7] Padovan, J., "Stresses in an Anisotropic Half Space," *AIAA Journal*, Vol. 11, No. 8, Aug. 1973, pp. 1194–1195.

[8] Padovan, J., "Thermoelasticity of an Elastic Anisotropic Half Space," *Proceedings of the Fourth Canadian Congress of Applied Mechanics*, Montreal, May 28–June 1, 1973, pp. 73–74.

[9] Flugge, W., *Stresses in Shells*, Springer-Verlag, New York, 1967, pp. 396–407.

Simple Spectroscopic Technique for the Arc Region of Plasma Accelerators

ROBERT P. COLLIER* AND DAVID S. SCOTT†
University of Toronto, Toronto, Ontario, Canada

Introduction

THE application of spectroscopic diagnostic techniques to plasma accelerator exhaust plumes is well known and documented.[1-6] However, the use of spectroscopy in the accelerator arc region has been quite limited. This results, primarily, from the lack of convenient optical access to the discharge region. One solution to this problem has been that of Grossman[7] who used an anode in which viewing ports had been drilled to obtain spectroscopic data yielding average temperature and density in the arc region. Bohn, Beth, and Nedder[2] have suggested a modified Abel inversion technique which allows transformation of data obtained at angles not perpendicular to the plasma axis.

Received June 13, 1973; revision received August 16, 1973.

Index categories: Plasma Dynamics and MHD; Electric and Advanced Space Propulsion; Radiation and Radiative Heat Transfer.

* Research Associate, Department of Mechanical Engineering. Student Member AIAA.

† Associate Chairman, Department of Mechanical Engineering.

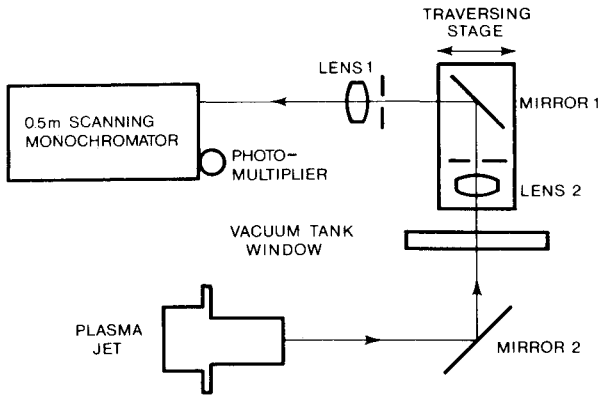

Fig. 1 Schematic of optical system.

Presumably, this method might be applied to the arc region. It is the purpose of this Note, however, to propose a simple technique which provides radial profiles of intensity in the arc region, without modification of the electrodes, and without need for numerical inversion of the measured data.

Analysis

The intensity observed by any spectral measuring device will include contributions from every point along the line of sight for the device. If a photomultiplier were arranged to view the accelerator arc region through the exhaust plume, the measured intensity would be modified by the emission and absorption of the plume, and the continuum emission from the hot cathode surface. Assuming self-absorption of the chosen spectral lines to be small, the measured intensity would be the value obtained by integrating the emission along the line of sight. If the distribution of emission along the line of sight through the plume were known and if the cathode emission were known, then these values could be subtracted from the total to obtain the contribution due to the plasma in the arc region. Thus, for an optically thin plasma, the absolute intensity of a line in the arc region may be written as

$$I_{\text{arc}} = \frac{1}{l_{\text{arc}}}\left[\frac{4\pi L\Delta\lambda}{S_{\text{cal}}}(S - S_{\text{cath}}) - \int I_{\text{plume}}\,dz\right] \qquad (1)$$

where L is the brightness of the calibration lamp, $\Delta\lambda$ is the wavelength band passed to the detector by the exit slit, S is the total signal current obtained by observing the arc region through the plume, S_{cath} is the signal current due to cathode continuum, l_{arc} is the length of arc region along the line of sight, and S_{cal} is the signal current due to the calibration lamp. If the contributions of the plume and the cathode continuum were small compared to that of the arc region, they could be neglected. Under these circumstances a radial profile of arc region intensity would be obtained directly by measuring total intensity as a function of radial position.

Table 1 Wavelengths used in this study, Angstroms

AI	AII	Continuum
4044.4	3850.6	3848.0
4158.6	4348.1	3897.0
4164.2	4379.7	4000.0
4198.3	4426.0	4196.5
4200.7	4609.6	4213.0
4272.2	4764.9	4396.5
4702.3	4806.1	4625.0
4708.4	4847.9	4852.0
5187.3	4879.9	5029.0
	5062.1	5238.5

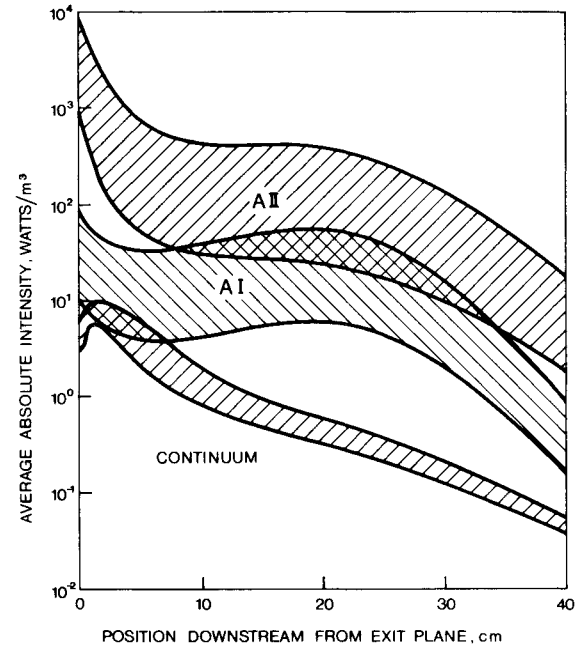

Fig. 2 Exhaust plume intensity as a function of position.

Experiment

An experiment was performed to measure the emission of the exhaust plume and its value relative to the arc region for a typical plasma accelerator. The accelerator was geometrically similar to those of Larson[8] and Shih,[9] although the cathode was

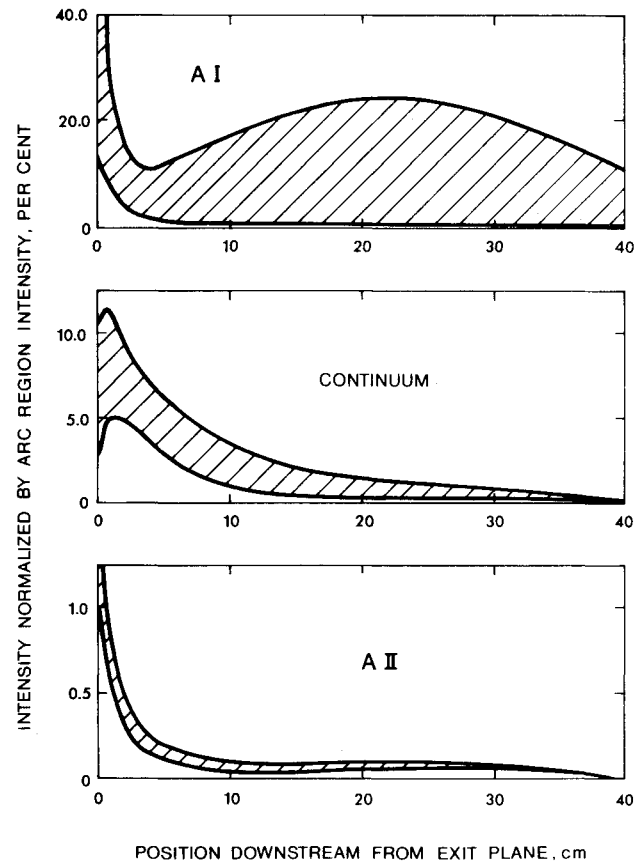

Fig. 3 Exhaust plume intensity, normalized by corresponding arc region value, as a function of position (note scale change).

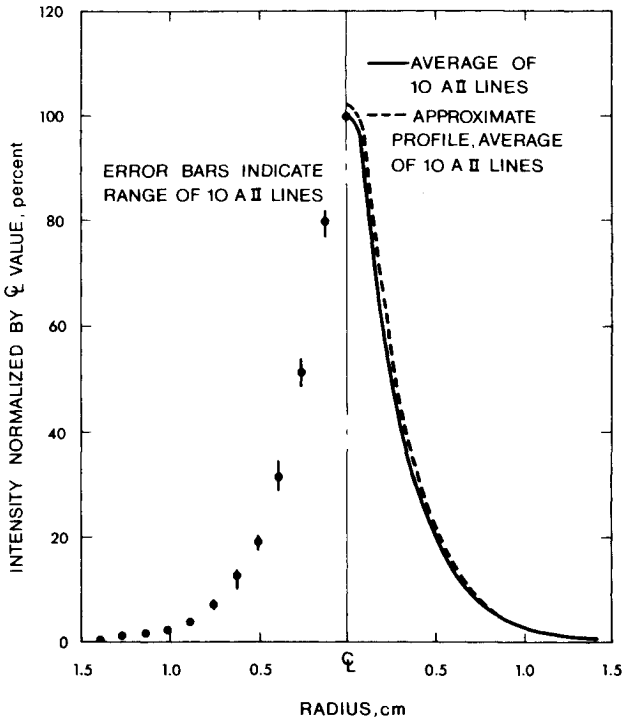

Fig. 4 Arc region intensity, normalized by centerline value, as a function of radial position.

modified slightly to provide improved cathode spot stability. All data were taken with an argon mass flow rate of 0.1 g/sec, background tank pressure of 7.5×10^{-2} torr, current of 125 amp at 20 v and zero applied magnetic field. A 0.5-m scanning monochromator with photomultiplier detector, front surface mirrors and achromatic lenses were used as shown in Fig. 1 to measure intensity integrated along the axial direction as a function of radial position. In addition, lateral intensities, integrated over the plume diameter, were measured at six stations downstream from the accelerator exit plane. The optical response of the system was calibrated before and after each run by replacing the source with a tungsten standard lamp.

Preliminary spectra were taken to aid in the choice of the representative spectral lines shown in Table 1. Ten AII lines, nine AI lines, and ten continuum values were chosen on the bases of representative strength, freedom from interference from other lines, freedom from self-absorption,[10-13] and positive source identification.

Results and Discussion

Results indicating the range of intensities measured in the plume are shown in Fig. 2, while profiles of absolute intensity normalized by the corresponding arc region value are shown in Fig. 3. Comparison of these two figures indicates that AII radiation dominates the arc region. Since the distribution of normalized AII plume intensity, shown in Fig. 3, exhibits so little scatter, it can be redefined in terms of the arc intensity which was used for normalization. This allows a simplification of Eq. (1) for the AII species, such that

$$I_{\text{arc}} = \frac{4\pi L \Delta\lambda}{S_{\text{cal}}} \frac{(S - S_{\text{cath}})}{(I_{\text{arc}} + F)} \tag{2}$$

where F is the integral of the normalized AII intensity distribution along the line of sight. This form makes it easy to visualize the error introduced by neglecting the radiation from the exhaust plume ($I_{\text{arc}} + F \simeq I_{\text{arc}}$) and the cathode ($S - S_{\text{cath}} \simeq S$).

An example of this error is indicated in Fig. 4, where a radial profile of AII arc intensity, normalized by the corresponding centerline value is shown, along with the approximate intensity profile obtained by neglecting the plume and cathode contributions in Eq. (2). The error introduced by this approximation ranges from 1.1% to 2.1% of the corrected value and is consistent for all AII lines measured.

For this typical plasma accelerator, the AII species dominates the arc region, and the AII intensity in the arc region is substantially higher than that of the exhaust plume or the corresponding continuum radiation from the cathode. Thus, the AII arc region intensity may be closely approximated by neglecting the plume and continuum contributions.

References

[1] Connolly, D. J. et al., "Low Environmental Pressure MPD Arc Tests," *AIAA Journal*, Vol. 6, No. 7, July 1968, pp. 1271–1276.

[2] Bohn, W. L., Beth, M.-U., and Nedder, G., "On Spectroscopic Measurements of Velocity Profiles and Non-Equilibrium Radial Temperatures in an Argon Plasma Jet," *Journal of Quantitative Spectroscopy and Radiative Transfer*, Vol. 7, 1967, pp. 661–676.

[3] Adcock, B. D., "Temperature Measurements on a Subatmospheric Argon Plasma Jet," *Journal of Quantitative Spectroscopy and Radiative Transfer*, Vol. 7, 1967, pp. 385–400.

[4] Freeman, M. P., "A Quantitative Examination of the LTE Condition in the Effluent of an Atmospheric Pressure Argon Plasma Jet," *Journal of Quantitative Spectroscopy and Radiative Transfer*, Vol. 8, 1968, pp. 435–450.

[5] Sovie, R. J. and Connolly, D. J., "A Study of the Axial Velocities in an Ammonia MPD Thruster," *AIAA Journal*, Vol. 7, No. 4, April 1969, pp. 723–725.

[6] Knopp, C. F., Gottschlich, C. F., and Cambel, A. B., "The Spectroscopic Measurement of Temperature in Transparent Argon Plasmas," *Journal of Quantitative Spectroscopy and Radiative Transfer*, Vol. 2, 1962, pp. 297–299.

[7] Grossman, W., Jr., "Theory and Experiment of a Coaxial Plasma Accelerator," Ph.D. thesis, 1964, Virginia Polytechnic Institute and State Univ., Blacksburg, Va., pp. 34–39.

[8] Larson, A. V., "Experiments on Current Rotations in an MPD Engine," *AIAA Journal*, Vol. 6, No. 6, June 1968, pp. 1001–1006.

[9] Shih, K. T., "Anode Current and Heat Flux Distribution in an MPD Engine," *AIAA Journal*, Vol. 8, No. 2, Feb. 1970, pp. 377–378.

[10] Olsen, H. N., "The Electric Arc as a Light Source for Quantitative Spectroscopy," *Journal of Quantitative Spectroscopy and Radiative Transfer*, Vol. 3, 1963, pp. 305–333.

[11] Malone, B. S. and Corcoran, W. H., "Transition Probability Measurements in the Blue-Near-U.V. Spectrum of Argon I," *Journal of Quantitative Spectroscopy and Radiative Transfer*, Vol. 6, 1966, pp. 443–449.

[12] Tourin, R. H., "Optically Thick Plasmas," *Journal of Quantitative Spectroscopy and Radiative Transfer*, Vol. 3, 1963, pp. 89–90.

[13] Tidwell, E. D., "Transition Probabilities of Argon II," *Journal of Quantitative Spectroscopy and Radiative Transfer*, Vol. 12, 1972, pp. 431–441.

On the Structure of Jet Plumes

JOHN H. FOX*
ARO, Inc., Arnold Air Force Station, Tenn.

Nomenclature

d_j = diameter of nozzle at exit plane
l = axial distance from nozzle exit to Mach disk
M_E = exit Mach number of nozzle
p_E = static pressure at nozzle exit
p_∞ = ambient pressure
S = diameter of Mach disk
x_b = axial distance from nozzle exit to body (Fig. 5)
γ = ratio of specific heats
θ_N = half-angle of nozzle exit
ω = axial distance from nozzle exit to intersection of reflected shock with plume boundary (primary wavelength)

Received June 15, 1973; revision received August 30, 1973.
Index category: Jets, Wakes, and Viscid-Inviscid Flow Interactions.
* Scientific Programmer.